

Spectral fluorescent study of Rhodamine 6G molecules embedded in different layers of one-dimensional polymer-based photonic crystals

© Yu.A. Strokova, A.M. Saletsky

Department of Physics, Moscow State University,
119991 Moscow, Russia

e-mail: strokova.yuliya@physics.msu.ru, sam@physics.msu.ru

Received 24.06.2022

Revised 11.10.2022

Accepted 12.10.2022

The spectral characteristics of the fluorescence of Rhodamine 6G (Rh6G) molecules doped into different layers of one-dimensional photonic crystals (PCs) have been studied at various detection angles. The studied PCs differ in the spectral position of the photonic band gap (PBG) with respect to the Rh6G luminescence spectrum. A computation method of the density of PC's electromagnetic modes have been proposed. The spectral characteristics of Rh6G fluorescence and computed relative density of electromagnetic modes versus the wavelength have been compared for different detection angles. The experimental and theoretical dependences demonstrate good agreement.

Keywords: Photonic crystals, photonic band gap, density of electromagnetic modes, spin-coating method, polymers, cellulose acetate, poly(N-vinylcarbazole), dye, Rhodamine 6G, fluorescence spectra.

DOI: 10.21883/EOS.2022.12.55240.3859-22

Introduction

With the creation of structures capable of modifying the local density of electromagnetic modes, it became possible to significantly change the spectral properties of luminophores embedded in such systems. Such structures include photonic crystals (PCs). In one-dimensional PCs, the local density of electromagnetic (EM) modes becomes dependent on the wavelength, direction and polarization of the radiation and the coordinates of the phosphor inside the crystal, which causes a change in the fluorescence spectra of the molecules embedded in the PCs. At the same time, the modified emission of luminophores in the PCs matrix can serve to create new effective light-collecting [1] and light-emitting devices [2], lasers [3–5], sensor applications [6]. In PCs, there is a change in the efficiency of electronic excitation energy transfer between embedded dye molecules of different types. Thus, in [7,8], the angular dependence of the efficiency of excitation energy transfer in a donor-acceptor pair of dye molecules was established, which is due to the depletion of available photonic modes for radiation decay of photonic crystal bandgap compared to a homogeneous medium and depending on the spectral position of the photonic stop zone of the photonic crystal.

One-dimensional polymer PCs manufactured by spin-coating method can serve as a matrix for almost any luminophores: organic dyes [9], quantum dots [10], J-aggregates [11], rare earth element complexes [12]. In addition, this method makes it possible to prepare a large number of varieties of these structures: photonic crystals without defects or with one or more defective layers, photonic crystals with variable layer thickness, etc.

The majority of experimental work testifies to the effective spectral and angular redistribution of radiation of luminophores embedded in the matrix of polymer PCs and photonic crystals with a defective layer [9,13], manufactured by spin-coating. The effect is observed for all types of luminophores [9–12]. In the work [3], a low-threshold surface-emitting laser with distributed feedback is implemented, which is a polymer PCs with a defective layer doped with a laser dye.

Despite a number of works devoted to the study of the fluorescent characteristics of dye molecules embedded in PCs based on polymer films, many issues remain unresolved. Thus, there is no comparison of the spectral characteristics of molecules embedded in PCs layers with a higher or lower refractive index, there is no information about the effect of a defective PCs resonator layer on spectral characteristics, there is no analysis of the conditions under which the greatest modification of fluorescence spectra is observed. The question of the relationship between the local density of the EM modes of PCs and the fluorescence spectra of embedded molecules is not fully clarified: is it possible to predict the luminophore luminescence spectra based on the known structure of the PCs, and, conversely, is it possible, by measuring the luminophore luminescence spectra in the PCs matrix, to accurately determine the local density of the EM modes, i.e., to use fluorescence spectroscopy to probe the properties of PCs.

In this paper, the fluorescence spectra of Rhodamine 6G (Rh6G) in three PCs were experimentally studied at different spectral positions of the photonic band gap (PBG) with respect to the dye spectrum at different angles of radiation detection. The local density of EM modes is calculated using the proposed method. On this basis, the

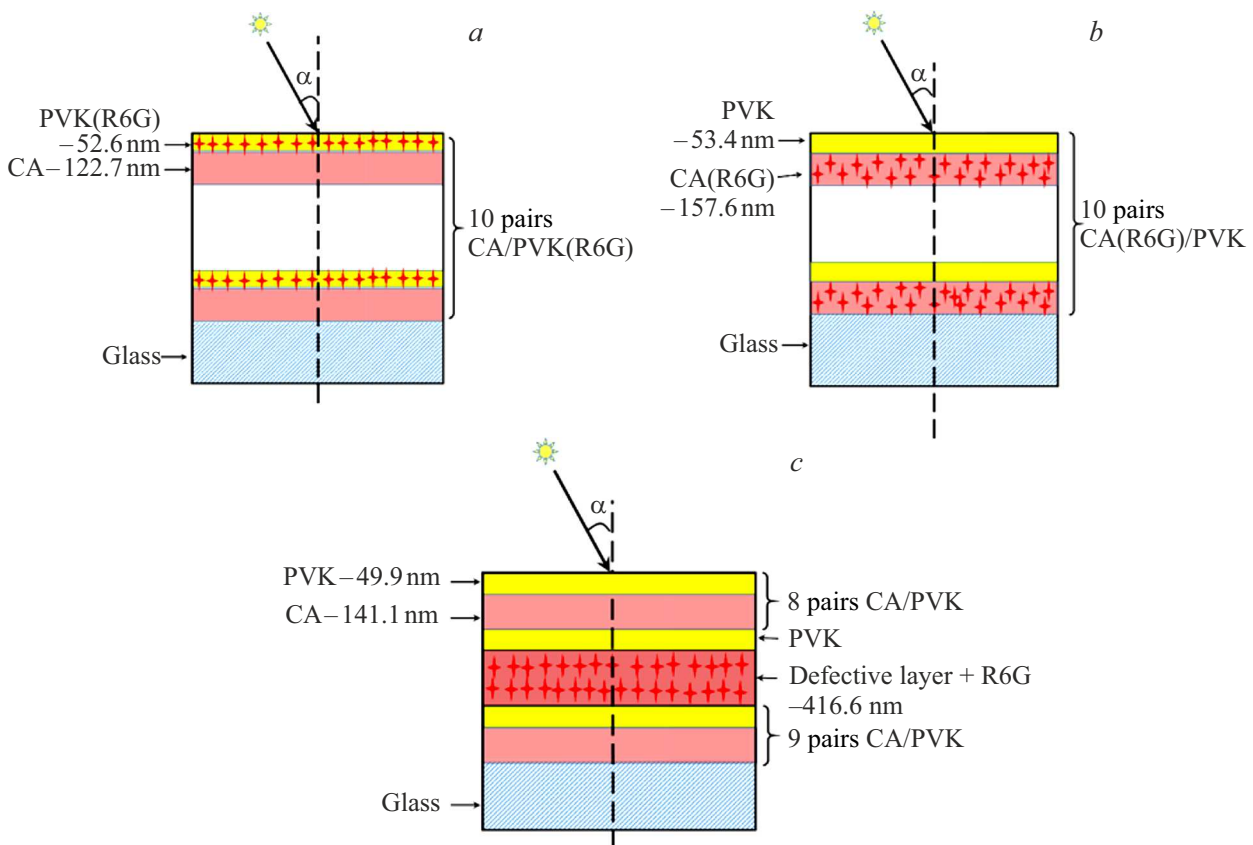


Figure 1. Structures PC1 (a), PC2 (b) and PC3 (c).

shape of the spectra of the phosphor fluorescence modified in the PCs matrix can be predicted quite accurately.

Materials and methods

To manufacture the one-dimensional PCs based on alternating polymer layers with different refractive index they used [14] cellulose acetate (CA, molecular weight 100,000, Across Organics, refractive index $n = 1.475$) and poly-N-vinylcarbazole (PVK, molecular weight 90,000, Across Organics, $n = 1.683$) and solvents diacetone alcohol and chlorobenzene, respectively. Three types of PCs samples were manufactured, further PC1, PC2 and PC3. CA solutions were prepared with concentrations of 3,g per 100,mL of solvent for PC1 and 3.535,g and 4.665,g per 100,mL of solvent for PC2, PC3. The concentration of PVK solution for all samples was the same and was 2.485 g per 100 mL of solvent. To completely dissolve CA in diacetone alcohol, the solution was kept at a temperature of 100°C for 90 min. The same solutions with a concentration of Rh6G 10^{-4} mol/L were prepared for the formation of PCs layers doped with dye.

The G3P Spincoat (Speciality Coating Systems) centrifuge was used to manufacture the films. Polymer solutions were applied dynamically to glass substrates $15 \times 15 \times 1$ mm ($n = 1.483$). After applying each two

layers of PVK and CA, the structure was kept at a temperature of 80°C for 2 min. The thickness of the polymer films was varied by changing the rotation frequency of the centrifuge. The following samples were prepared: PC1 — $(\text{PVK}(\text{Rh6G})/\text{CA})_{10}$, PC2 — $(\text{PVK}/\text{CA}(\text{Rh6G}))_{10}$, PC3 — $(\text{PVK}/\text{CA})_8/\text{PVK}/\text{CA}_{\text{def}}(\text{Rh6G})/(\text{PVK}/\text{CA})_9$. In PC1, all PVK layers are doped with Rh6G, in PC2 — all CA layers, in PC3 — CA_{def} layer. The structure of the manufactured PCs samples is shown in Fig. 1. The thicknesses of the PCs layers shown in Fig. 1 are determined as a result of the approximation of the transmission spectra by the dependencies $T(\lambda)$.

The luminescence spectra of Rh6G in the PCs were compared with the dye spectra in triple polymer films prepared under the same conditions as PCs: $\text{CA}/\text{PVK}(\text{Rh6G})/\text{CA}$ — for PC1, $\text{CA}(\text{Rh6G})/\text{PVK}/\text{CA}(\text{Rh6G})$ — for PC2, $\text{CA}/\text{PVK}/\text{CA}_{\text{def}}(\text{Rh6G})$ — for PC3.

Transmission and reflection spectra were measured for the manufactured samples at different angles of incidence of light and for TE- or TM-polarizations (spectrophotometer PB 2201 with a prefix for measuring the reflection coefficient, Solar).

Steady-state spectra of Rh6G in PCs were measured at different detection angles and TE- and TM-polarizations on the experimental setup, the block diagram of which is shown in Fig. 2. The excitation of the sample (5) was

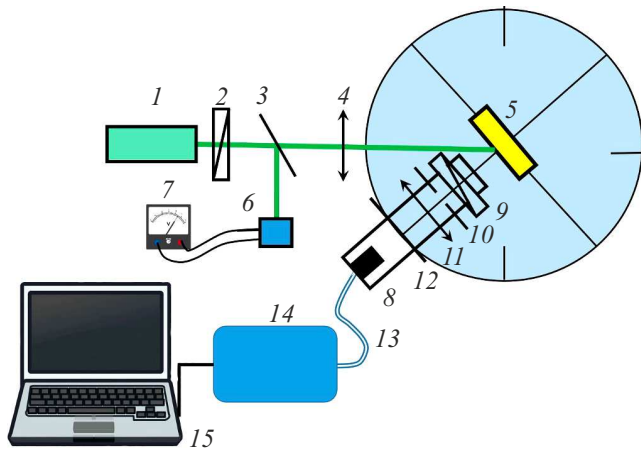


Figure 2. Experimental setup scheme.

carried out by a laser (1) with a wavelength of 505 nm (OxLaser), the radiation of which was passed through a polarizer (2), a dividing plate (3) and the lens (4). Reception of the fluorescence signal was carried out by a light guide (13), in front of which a collecting lens (11), an aperture (10) limiting the luminescence collection angle $\pm 2.5^\circ$, a polarizer (9) and color glass filter, which cuts off the excitation wavelength were installed. Luminescence was recorded using a spectrometer (14) based on a CCD array (Spectrometer LD/HD, 3B Scientific GmbH) and a computer (15). Fluorescence spectra were recorded at different angles (due to the rotation of the platform (8)). To measure and control the intensity of laser radiation, a part of it was directed to a photodetector (3) using a dividing plate (6) and recorded with a millivoltmeter (7). Luminescence spectra of reference samples (Rh6G in triple polymer films) were also measured.

Results and discussion

Fig. 3 shows the transmission spectra of the studied PCs measured at 0° . From Fig. 3 it can be seen that for PC1, the PBG occupies a wavelength range of 488–594 nm, for PC2 — 582–702 nm, for PC3 — 534–638 nm with a defective mode at 577 nm. The same figure shows the fluorescence and absorption spectra of Rh6G in a CA film. From Fig. 3 it can be seen that for PC1 with the fluorescence spectrum of the dye, the long-wave edge of the PBG overlaps, for PC2 — the short-wave edge of the PBG, for PC3 — the defective mode.

The transmission spectra of the studied PCs depend on the angle of their registration α . Fig. 4 shows the transmission spectra of PCs at different detection angles and TE polarization. From Fig. 4 it can be seen that with an increase in the registration angle α there is a short-wave shift of the transmission spectrum and a decrease in the transmission coefficient of T for the PBG. At the same time, for PC3 with α increasing a short-wave shift of the position

of the defective mode λ_{\max} is observed (Fig. 4, c). Fig. 4, d shows the dependences of the PBG maxima (λ_{PBG}) for PC1 (curve 1) and PC2 (curve 2) and the wavelength of the defective mode λ_{\max} for PC3 (curve 3) from the registration angle α . With increasing the registration angle α the position of the PBG changes.

Let us consider the fluorescence spectra of Rh6G molecules embedded in different types of PCs for different angles of light registration (Fig. 5).

For luminescence spectra of Rh6G embedded in polymer layers with a higher refractive index (PC1) (Fig. 5, a), with an angle α from 0 increasing to 40° a short-wave shift of the maximum of the luminescence spectrum is observed, because the long-wave edge of the PBG passes through the luminescence spectrum. At an angle of 50° , the PBG appears outside the luminescence spectrum. For the spectra of Rh6G molecules embedded in polymer layers with a lower refractive index (PC2) (Fig. 5, b), a long-wave shift of the spectrum is observed at $\alpha = 20^\circ$, and at $\alpha = 30\text{--}40^\circ$ — short-wave shift caused by passing of the short-wave edge of the PBG, while the long-wave part of the spectrum is suppressed by the PBG, and at $\alpha = 50^\circ$ the entire spectrum of Rh6G is suppressed. PC3 is distinguished by a large number of periods and, consequently, by the most pronounced features of the local density of EM modes. The Rh6G fluorescence spectrum in the defective PC3 layer splits into three bands (Fig. 5, c) due to the defective mode, short-wave and long-wave edges of the PBG. With an increase in the detection angle, a short-wave shift of all the luminescence bands occurs, repeating the short-wave shift of the wavelengths of the defective mode and the edges of the PBG for PC3, which are depicted by a dashed line in Fig. 5, c. From the insertion in Fig. 5, c it can be seen that the shift of the maximum of the middle luminescence band almost completely coincides with the dashed line, while the maxima of the outside luminescence bands are shifted relative to the dashed lines towards the true maximum of the luminescence spectrum Rh6G.

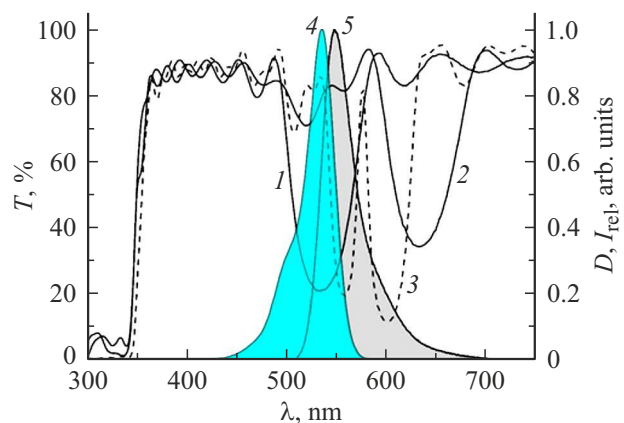


Figure 3. Transmission spectra at normal light incidence: PC1 (1), PC2 (2), PC3 (3). Curves 4 and 5 — absorption and fluorescence spectra of Rh6G in a polymer film (the film thickness $d = 1 \mu\text{m}$, $C_{\text{Rh6G}} = 5 \cdot 10^{-5} \text{ mol/l}$).

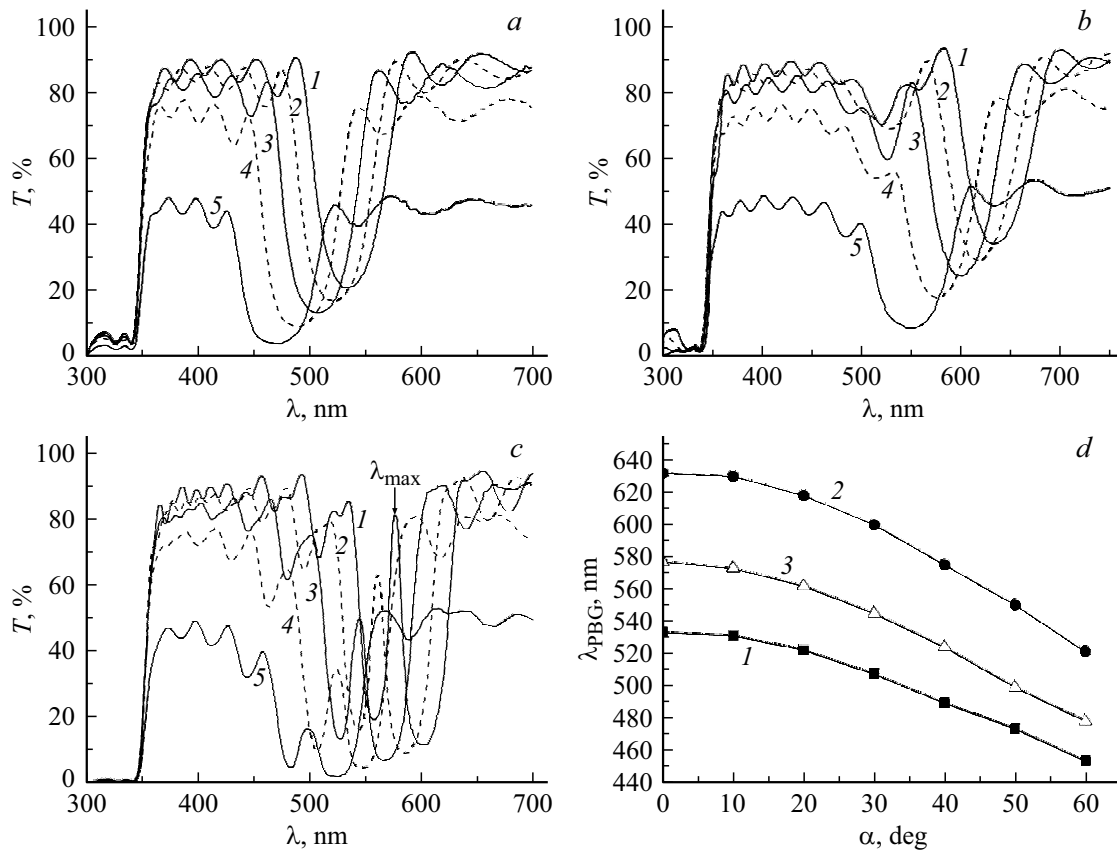


Figure 4. Transmission spectra of PC1 (a), PC2 (b), PC3 (c) at registration angles α : 0° (1), 20° (2), 30° (3), 40° (4) and 50° (5). Wavelength dependence λ_{PBG} (d) from the angle α .

Let us compare the spectral characteristics of Rh6G fluorescence in PCs with the relative density of EM modes in the crystal. To analyze changes in the fluorescence spectra of Rh6G in PCs, the relative fluorescence intensity $\frac{I}{I_0}(\lambda)$ was determined, where I — the fluorescence intensity of Rh6G in PCs, I_0 — the fluorescence intensity of Rh6G in comparison samples.

We determine the position of the EM modes ρ in the matrix of a one-dimensional PCs. We determine the dependence of the density of EM modes ρ on the wavelength in the matrix of one-dimensional PCs. It is known [15] that the probability of transition of a quantum system from an excited state with energy E_1 to a state with energy E_0 by spontaneous emission of a photon is equal to

$$\gamma_{10}^{\text{rad}} = \frac{2\pi}{\hbar} \rho(\omega) |\langle E_0, 1 | H_{\text{int}} | E_1, 0 \rangle|^2, \quad (1)$$

where $\langle E_0, 1 |$ — the final state of the substance-field system (nonexcited atom and 1 photon), $|E_1, 0\rangle$ — the initial state (excited atom, no photon) of the system, H_{int} — interaction Hamiltonian, $\rho(\omega)$ — the density of EM modes in the vicinity of the molecule.

In the matrix of a one-dimensional PC, the density of the EM modes ρ available for radiation becomes a function of the transition frequency ω , coordinates z_M of the dipole inside the PCs, radiation directions \mathbf{k} and dipole orientations

$\mathbf{e}_l - \rho(\omega, z_M, \mathbf{k}, \mathbf{e}_l)$. Hence, the probability of spontaneous emission $\gamma_{10}(\omega, z_M, \mathbf{k}, \mathbf{e}_l)$ also becomes a function of these variables.

The luminescence intensity measured in the number of photons depends on the probabilities of electron-vibrational transitions of molecules and the population of the initial electron-vibrational level. The total rate of transition of molecules from the excited state to the non-excited state consists of the rate of radiative transitions mentioned above and the rate of non-radiative transitions, which in turn can be divided into transitions due to the internal conversion of excited molecules and transitions due to interaction with the medium [16]. The quantum yield of Rh6G fluorescence is close to unity, so nonradiative transitions due to internal conversion can be neglected. Since the considered polymer medium does not have absorption in the spectral region of Rh6G radiation, the rate of transitions due to interaction with the medium can also be neglected.

Under stationary excitation provided that the molecular system is far from saturation, the population of the excited electron-vibrational level N_1 becomes a constant value [17], and the luminescence intensity is defined as $I(\omega, z_M, \mathbf{k}, \mathbf{e}_l) = \gamma_{10}(\omega, z_M, \mathbf{k}, \mathbf{e}_l) N_1$. Therefore, taking into account the formula (1) the luminescence intensity is directly proportional to the local EM mode density.

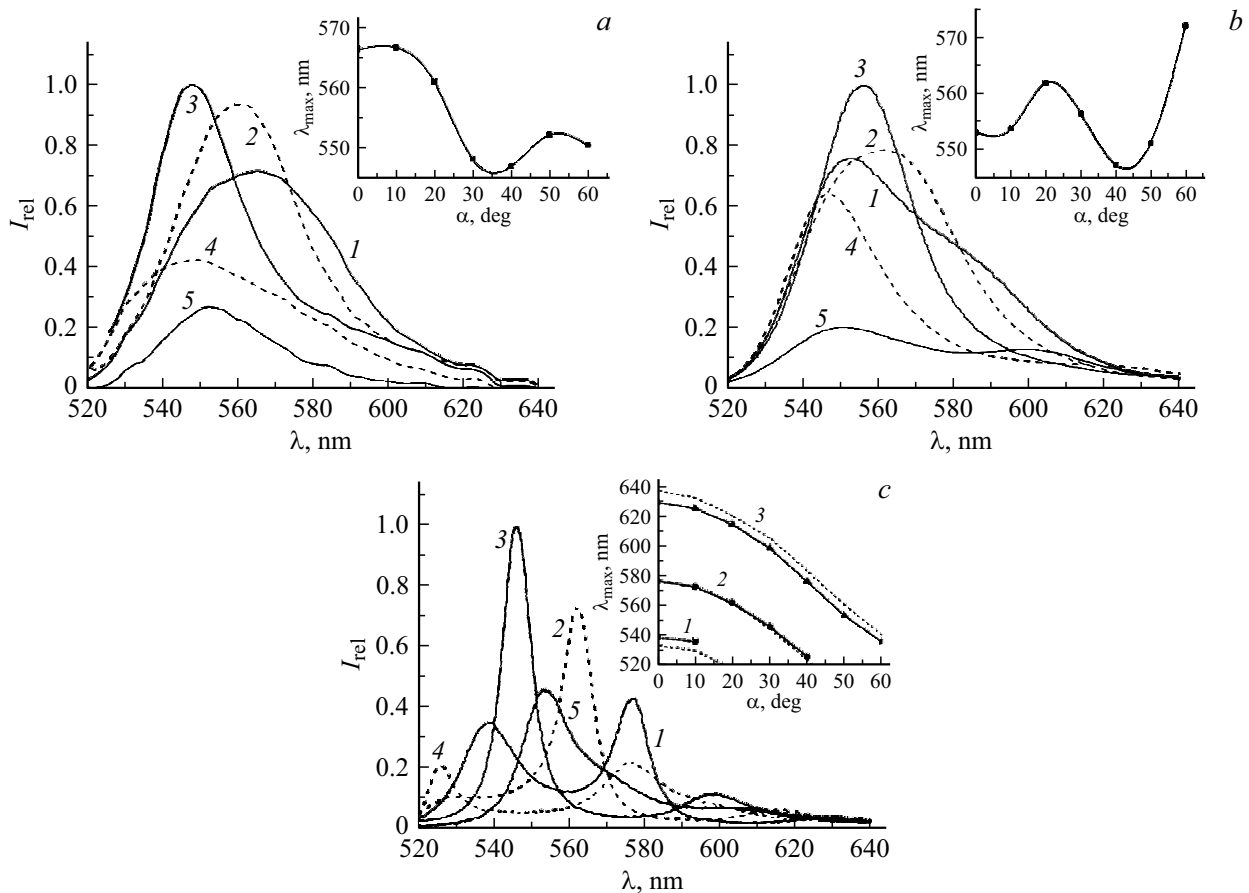


Figure 5. Normalized fluorescence spectra of Rh6G in PC1 (a), PC2 (b) and PC3 (c) at different registration angles α : 0° (1), 20° (2), 30° (3), 40° (4) and 50° (5). The inserts show the dependence of the wavelength of the maxima of the fluorescence spectra of Rh6G on α .

In this regard, the modification of the local density of EM modes should lead to a proportional redistribution of the intensity of the luminescence spectrum in frequency, radiation direction, coordinate and orientation of the dipole inside the PCs. The measured luminescence signal is common to all PCs layers containing a dye, so the intensity dependence on the dipole coordinate cannot be established in such an experiment. The dependence of the luminescence intensity on the two orientations of the dipoles was established by measuring TM- and TE-polarized luminescence.

Within the framework of the dipole approximation, we estimate the local density of EM modes. In the work [18] it is shown that for a dipole current source $\mathbf{J}(\mathbf{x}) = \mathbf{e}_l \delta(\mathbf{x} - \mathbf{x}_0)$ located at the point \mathbf{x}_0 , where \mathbf{e}_l is a unit vector in the direction of $l \in \{1, 2, 3\}$, the local density of EM modes available for radiation can be found by the formula

$$\rho_l^{\text{rad}}(\mathbf{x}_0, \omega) = \frac{4}{\pi} P_l(\mathbf{x}_0, \omega), \quad (2)$$

where $P_l(\mathbf{x}_0, \omega)$ — the power emitted by $\mathbf{J}(\mathbf{x}) = \mathbf{e}_l \delta(\mathbf{x} - \mathbf{x}_0) e^{-i\omega t}$. Thus, the local density of EM modes is directly proportional to the power emitted by the l -oriented dipole source.

Since the spectral characteristics were measured depending on the wavelength, then we will talk about the dependence of the luminescence intensity and the local density of EM modes on the wavelength, meaning the wavelength in vacuum.

In the work [19], a formalism is proposed for calculating the Umov-Poynting vector of a field in a layer N created by a dipole placed in the M th layer of a plane-layered structure. Dipole far-field radiation can be represented as the sum of plane waves, and the electric and magnetic fields of each plane wave can be calculated by the transfer matrix method. If the refractive indices of the layers N and M coincide, respectively, in the PCs and the reference sample, then the ratio of the average Umov-Poynting vectors in the PCs and the reference is the ratio of the average squares of electric fields.

We note that the solution for the mean square of the electric field in the layer $N \langle E_N^2 \rangle$, found according to [19], will not change if you change the direction of wave propagation to the opposite (from layer N to layer M) and define $\langle E_M^2 \rangle$ in layer M . This method of calculating $\langle E^2 \rangle$ is more convenient for cases when the phosphor is contained in a layer or layers of finite thickness, since it

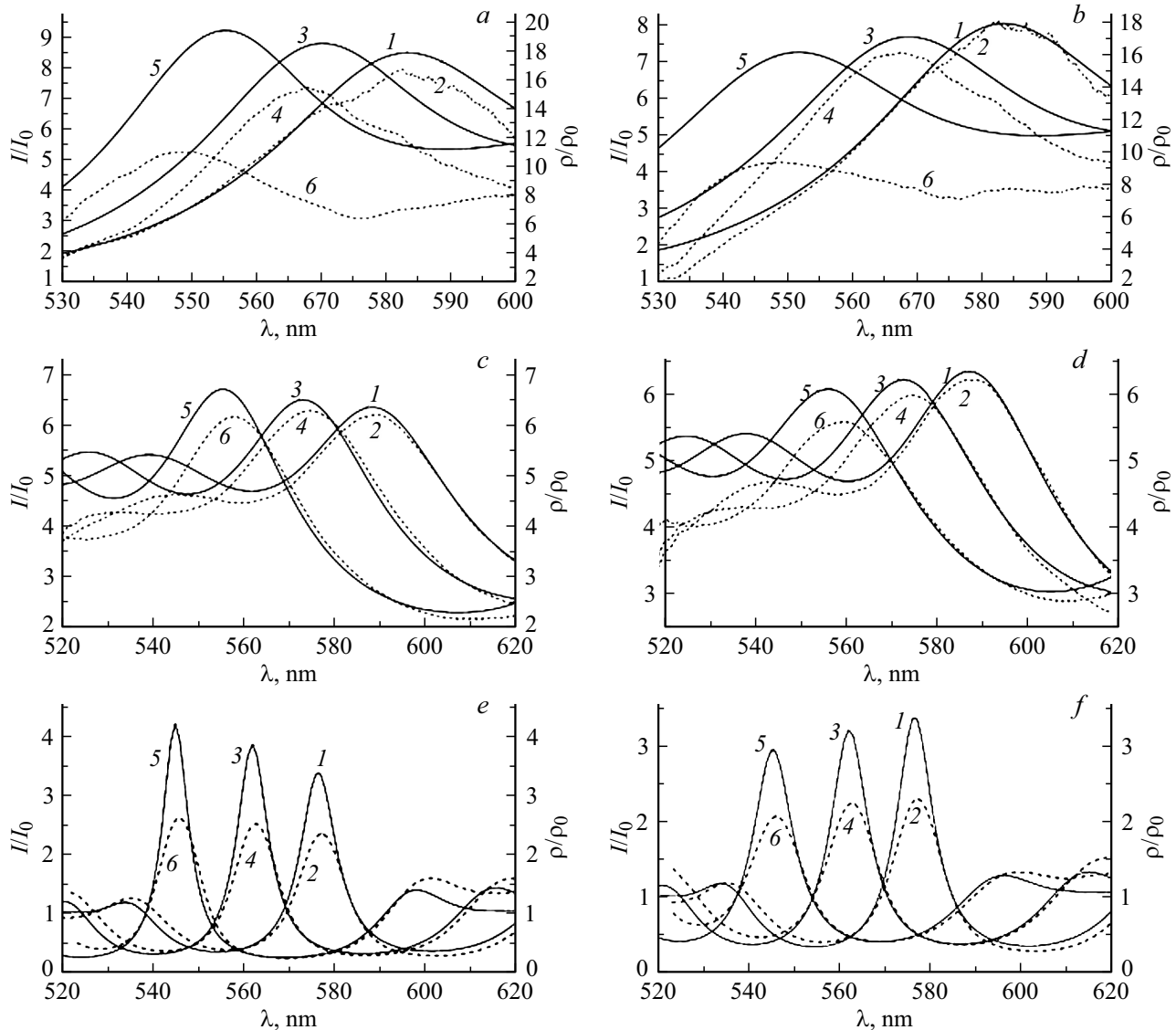


Figure 6. Spectral dependencies I/I_0 (2, 4, 6) and ρ/ρ_0 (1, 3, 5) at the registration angles $\alpha = 0^\circ$ (1, 2), 20° (3, 4) and 30° (5, 6) for TE- (a, c, e) and TM-polarizations (b, d, f) for PC1 (a, b), PC2 (c, d) and PC3 (e, f).

allows you to calculate the average square of the field in the entire structure depending on the coordinate z and perform integration over layers containing the phosphor:

$$\langle E^2(\lambda, \mathbf{k}, \mathbf{e}_l) \rangle_{\text{int}} = \sum_i \int_{z_{i,\text{begin}}}^{z_{i,\text{end}}} \langle E^2(\lambda, z, \mathbf{k}, \mathbf{e}_l) \rangle dz, \quad (3)$$

where layers i — are layers containing phosphor, $z_{i,\text{begin}}$ and $z_{i,\text{end}}$ — coordinates of the beginning and end of the i th layer.

The time average square of the electric field depending on the coordinate z was calculated according to [20]. Integral density of EM modes, common to all layers with dye and normalized to the integral density of EM modes in the

reference sample,

$$\frac{\rho^{\text{rad}}(\lambda, \mathbf{k}, \mathbf{e}_l)}{\rho_0^{\text{rad}}(\lambda, \mathbf{k}, \mathbf{e}_l)} = \frac{\langle E^2(\lambda, \mathbf{k}, \mathbf{e}_l) \rangle_{\text{int}}}{\langle E_0^2(\lambda, \mathbf{k}, \mathbf{e}_l) \rangle_{\text{int}}}. \quad (4)$$

From the resulting formulas given in [19], it follows that the Umov-Poiting vector can be calculated for each component (TM and TE) of the dipole separately. In the case of calculating the square of the field of an incident wave in a layered structure, this corresponds to incident TM- and TE-polarized waves.

It is known [21] that the energy density of the incident EM wave is distributed unevenly across the PCs layers and depends on the frequency (wavelength). The energy density of a wave with a length more than PBG is concentrated in layers with a higher refractive index, and, conversely, the energy density of a wave with a length

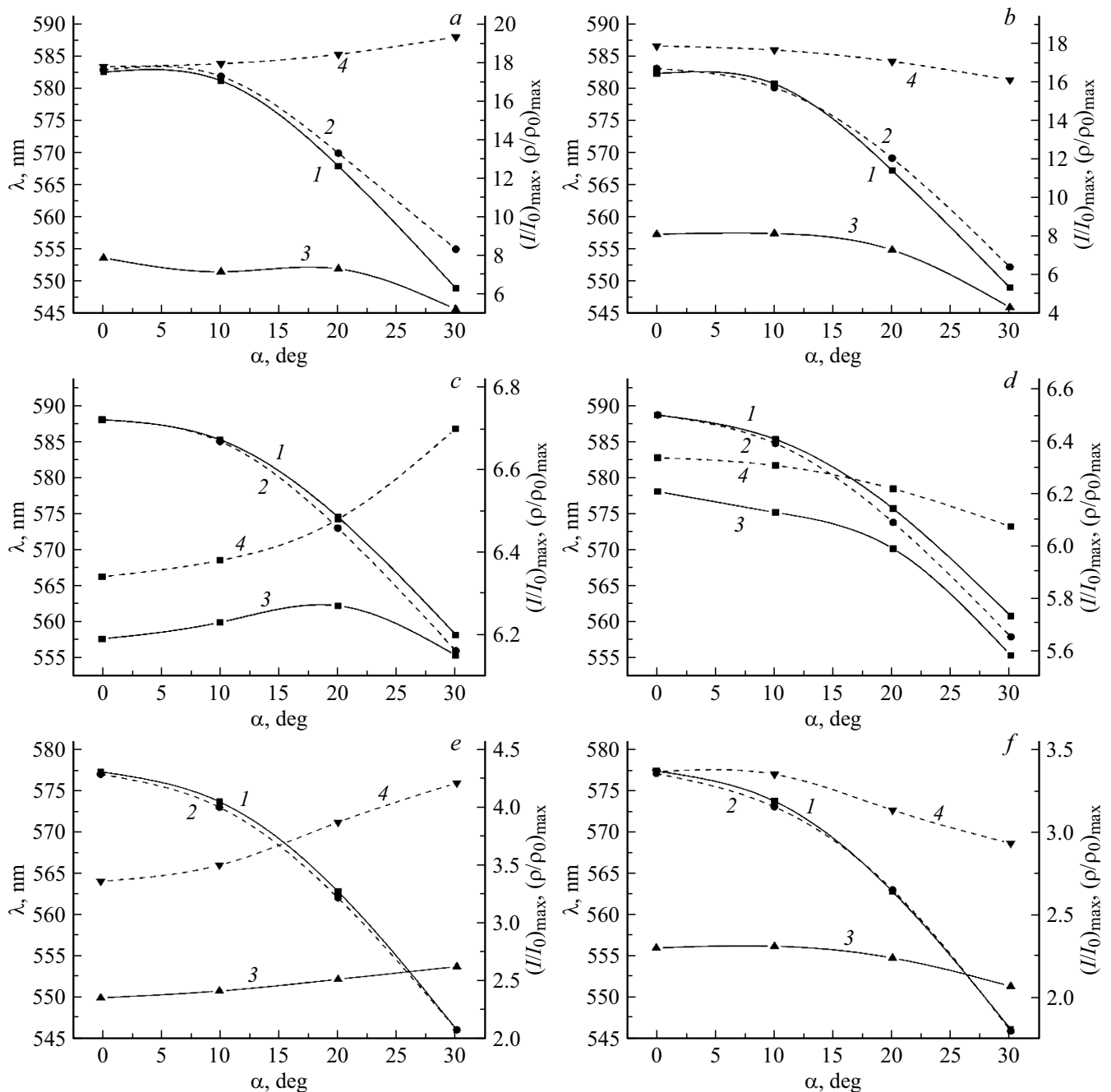


Figure 7. Dependence of wavelength (curves 1, 2) and absolute values of maximum (curves 3, 4) of dependencies $\frac{I}{I_0}(\lambda)$ (curves 1, 3) and $\frac{\rho}{\rho_0}(\lambda)$ (curves 2, 4) on the registration angle α for three types of PCs (PC1 — a, b; PC2 — c, d; PC3 — e, f) and two polarizations (TE-polarization — a, c, e; TM-polarization — b, d, f).

less than the PBG is concentrated in layers with a lower refractive index. Consequently, we can expect a change in the spectral-fluorescent characteristics of dye molecules embedded in layers where the energy density of the wave is concentrated.

Fig. 6 shows the dependences of the relative fluorescence intensity Rh6G $\frac{I}{I_0}(\lambda)$ and the relative EM density $\frac{\rho}{\rho_0}(\lambda)$, calculated using (4), for the three types of PCs studied and for the three angles of radiation detection: 0°, 20° and 30°.

Fig. 7 shows the dependences of the maximum wavelength of the curves $\frac{I}{I_0}(\lambda)$ and $\frac{\rho}{\rho_0}(\lambda)$ and the intensities at the maximum of these dependencies on the registration angle α for three types of PCs.

Let us first consider the obtained theoretical dependencies $\frac{\rho}{\rho_0}(\lambda)$. Since the calculation of $\rho_0(\lambda)$ is made for reference samples containing one layer with dye for PC1 and PC3 and 2 layers for PC2, then the value of $\frac{\rho}{\rho_0}(\lambda)$ away from the features caused by the PBG, tends to 10 for PC1, 5

for PC2 and 1 for PC3. The values of $\frac{\rho}{\rho_0}(\lambda)$, more than these values, indicate an increase in luminescence, and less than — to suppress the luminescence of the dye.

With the registration angle increasing, a short-wave shift of the dependence maximum of $\frac{\rho}{\rho_0}(\lambda)$ is observed, while for TE-polarization, the maximum value of $\frac{\rho}{\rho_0}(\lambda)$ grows with increasing angle α , and for TM-polarization — falls (see curves 1, 3, 5 in Fig. 6 and the curve 2 in Fig. 7). In the dependency $\frac{\rho}{\rho_0}(\lambda)$ for PC1 calculated for layers with a high refractive index, the luminescence amplification region corresponding to the long-wave edge of the PBG is noted; in the same dependence for PC2 calculated for layers with a low refractive index, — the amplification region corresponding to the short-wave edge of the PBG. In the dependence $\frac{\rho}{\rho_0}(\lambda)$ for PC3 calculated for the defective layer, there is an increase in the region of the defective mode and a slight increase at the edges of the PBG.

Let us compare the theoretical dependencies of $\frac{\rho}{\rho_0}(\lambda)$ with experimental $\frac{I}{I_0}(\lambda)$. For PC1 values $\frac{I}{I_0}(\lambda)$ at $\alpha = 0^\circ$ 2.3 times lower than the predicted calculations, this difference increases with increasing detection angle. A weak signal of Rh6G luminescence in PVK layers in PC1 may be associated with repeated heating of the structure during its preparation. There is a suppression of the short-wave part of the luminescence spectrum due to the intersection with the PBG, and an amplification of the spectrum occurring at the long-wave edge of the PBG. The wavelength of the dependence maximum $\frac{I}{I_0}(\lambda)$ coincides with the wavelength of the dependence maximum $\rho(\lambda)/\rho_0(\lambda)$ only for $\alpha = 0^\circ$, with the detection angle increasing, there is a shift of the maximum $\frac{I}{I_0}(\lambda)$ towards short wavelengths for two polarizations (curves 1, 2 in Fig. 7, a, b).

For PC2, suppression of the long-wave part of the luminescence spectrum and amplification due to the short-wave edge of the PBG are observed. We note the coincidence of the wavelength of the maximum of the dependence $\frac{I}{I_0}(\lambda)$ with the maximum for $\frac{\rho}{\rho_0}(\lambda)$ at $\alpha = 0^\circ$ for two polarizations; with increasing angle α the maxima of $\frac{I}{I_0}(\lambda)$ are shifted towards longer wavelengths relative to the maxima of $\frac{\rho}{\rho_0}(\lambda)$ (see curves 1, 2 in Fig. 7, c, d). In the angle range $0-20^\circ$, there is an increase in the values of the maximum relative luminescence intensity, and after 20° , the maximum value decreases, while the dependence $\frac{\rho}{\rho_0}(\lambda)$ predicts the growth of maximum values in the entire range of angles α (curves 3, 4 in Fig. 7, c). For TM-polarization, the maximum value of the dependence $\frac{I}{I_0}(\lambda)$ falls with increasing angle faster than the theory predicts (curves 3, 4 in Fig. 7, d).

A comparison of the dependencies for PC3 shows that the wavelength of the central peak coincides well with the calculated one at all angles for TE- and TM-polarization (curves 1, 2 in Fig. 7, e, f), while the value of the central maximum $\frac{I}{I_0}(\lambda)$ is 70% of the maximum of the dependence of $\frac{\rho}{\rho_0}(\lambda)$, and the values of the side peaks are slightly higher than predicted by the theory. It is necessary to additionally check the possibility of such excitation of luminescence in

the sample, in which the absolute values of the maxima of the experimental and theoretical dependences will coincide. With increasing angle α there is an increase in the values of the central maxima of the relative luminescence intensity for TE-polarization, however, lagging behind the calculated ones (curves 3, 4 in Fig. 7, e); for TM-polarization, there is a decline in the values of the maxima of the relative intensity, on the contrary, is lagging behind the calculated ones (curves 3, 4 in Fig. 7, f). The maxima of relative intensity caused by the edges of the PBG are shifted relative to those predicted by the theory towards longer wavelengths.

In general, for all PCs samples, experimental dependences of relative intensity $\frac{I}{I_0}(\lambda)$ agree well with the calculated dependencies $\frac{\rho}{\rho_0}(\lambda)$. For all samples, the wavelengths of the maxima of the experimental and calculated dependences coincide at a detection angle of 0° , for larger angles for PC1 and PC2 and minor maxima for PC3, a deviation from the calculated dependences towards larger or smaller wavelengths is observed. For PC1 and PC2, the best coincidence of experimental and calculated dependencies is observed near the PBG, with the distance from the PBG and its edges, the dependence subsidence is observed $\frac{I}{I_0}(\lambda)$ compared to $\frac{\rho}{\rho_0}(\lambda)$. Due to the large number of layers in PC3, the experimental dependence $\frac{I}{I_0}(\lambda)$ has the most significant features, expressed, however, to a lesser extent than predicted by theory.

The proposed method for comparing the experimental dependence of $\frac{I}{I_0}(\lambda)$ and calculated $\frac{\rho}{\rho_0}(\lambda)$ takes into account the change in the luminescence intensity of the dye due to a change in the rate of radiative transitions in the PCs matrix compared to the reference sample under the influence of a modified local density of propagating EM modes. Differences in experimental and calculated dependences indicate that other processes are also modified in the PCs matrix, in particular, the process of energy migration between molecules, which, firstly, affects the rate of non-radiative transitions (in the case of heterogeneously broadened spectra in the region of overlap of the luminescence spectrum with the absorption spectrum), and secondly, redistributes excited molecules in the region of transitions of lower energies. In general, the modified process of energy migration can lead to a redistribution of the intensity of the luminescence spectrum.

Conclusion

Thus, the presented results of an experimental study of the spectral-fluorescent characteristics of Rh6G show the possibility of modifying the fluorescence spectra of dye molecules during selective doping into various layers of polymer PCs manufactured by spin-coating. The comparison of the fluorescence spectra of Rh6G with the calculated (according to the method proposed in the work) dependence of the EM mode density on the wavelength and for different angles of radiation registration is carried out.

Experimental and theoretical dependencies demonstrate a good coincidence. In the defective layer of PC3, the fluorescence spectrum of Rh6G consists of three bands, the short-wave shift of which occurs with an increase in the detection angle.

Funding

The research was carried out within the framework of the activities of the Scientific and educational school of Lomonosov Moscow State University „Photonic and quantum technologies. Digital medicine“.

Conflict of interest

The authors declare that they have no conflict of interest.

References

- [1] G. Iasilli, R. Francischello, P. Lova, S. Silvano, A. Surace, G. Pesce, M. Alloisio, M. Patrini, M. Shimizu, D. Comoretto, A. Pucci. *Mater. Chem. Front.* **3**, 429 (2019). DOI: 10.1039/c8qm00595h
- [2] L. Hou, Q. Hou, Y. Mo, J. Peng, Y. Cao. *Appl. Phys. Lett.*, **87** (24), 243504 (2005). DOI: 10.1063/1.2119416
- [3] H. Sakata, H. Takeuchi, K. Natsume, S. Suzuki. *Opt. Express.*, **14** (24), 11681 (2006). DOI: 10.1364/OE.14.011681
- [4] H. Sakata, K. Yamashita, H. Takeuchi, M. Tomiki. *Appl. Phys. B*, **92**, 243 (2008). DOI: 10.1007/s00340-008-3082-7
- [5] A. Inoue, J. Hayashi, T. Komikado, S. Umegaki. *Opt. Lett.*, **32** (19), 2807 (2007). DOI: 10.1364/OL.32.002807
- [6] P. Lova, H. Megahd, D. Comoretto. *EPJ Web of Conferences*, **230**, 00007 (2020). DOI: 10.1051/epjconf/202023000007
- [7] Yu.A. Strokova, S.E. Svyakhovskii, A.M. Saletsky. *Opt. and Spectrosc.*, **125** (2), 208 (2018). DOI: 10.1134/S0030400X18080222.
- [8] Yu.A. Strokova, S.A. Svyakhovskiy, A.M. Saletsky. *J. Applied Spectroscopy*, **85** (6), 1013 (2019). DOI: 10.1007/s10812-019-00752-1.
- [9] F. Scotognella, A. Monguzzi, M. Cucini, M. Feinardi, D. Comoretto, R. Tubino. *International Journal of Photoenergy*, **2008**, 389034 (2008). DOI: 10.1155/2008/389034
- [10] V.M. Menon, M. Luberto, N.V. Valappil, S. Chatterjee. *Opt. Express.*, **16** (24), 19535 (2008). <https://doi.org/10.1364/OE.16.019535>
- [11] P. Lova, V. Grande, G. Manfredi, M. Patrini, S. Herbst, F. Würthner, D. Comoretto. *Adv. Optical Mater.*, **5** (20), 1700523 (2017). DOI: 10.1002/adom.201700523
- [12] P. Lova, M. Olivieri, A. Surace, G. Topcu, M. Emirdag-Eanes, M.M. Demir, D. Comoretto. *Crystals*, **10** (4), 287 (2020). DOI: 10.3390/cryst10040287
- [13] L. Frezza, M. Patrini, M. Liscidini, D. Comoretto. *J. Phys. Chem. C.*, **115** (40), 19939 (2011). DOI: 10.1021/jp206105r
- [14] T. Komikado, S. Yoshida, S. Umegaki. *Appl. Phys. Lett.*, **89** (6), 061123 (2006). <https://doi.org/10.1063/1.2336740>
- [15] S.V. Gaponenko, N.N. Rozanov, E.L. Ivchenko, A.V. Fedorov, A.V. Baranov, A.M. Bonch-Bruevich, T.A. Vartanyan, S.G. Przybelski. *Optics of nanostructures* (Nedra, St. Petersburg, 2005).
- [16] R. Carminati, A. Cazé, D. Cao, F. Peragut, V. Krachmalnicoff, R. Pierrat, Y.De. Wilde. *Surface Science Reports.*, **70** (1), 1 (2015). DOI: 10.1016/j.surfrep.2014.11.001
- [17] L.V. Levshin, A.M. Saletsky. *Luminescence and its Measurements* (Moscow University Press, Moscow, 1989).
- [18] *Advances in FDTD computational electrodynamics: photonics and nanotechnology*, ed. by A. Taflove, A. Oskooi, S.G. Johnson (Artech House, Boston, 2013).
- [19] N. Calander. *J. Phys. Chem. B*, **109** (29), 13957 (2005). DOI: 10.1021/jp0510544
- [20] W.N. Hansen. *J. Opt. Soc. Am.*, **58** (3), 380 (1968). DOI: 10.1364/JOSA.58.000380
- [21] J.D. Joannopoulos, S.G. Johnson, J.N. Winn, R.D. Meade. *Photonic Crystals: Molding the Flow of Light*, 2nd ed. (Princeton University Press, Princeton, 2011).